Experimental Investigation of Leading-Edge Tubercled Hydrofoils attached to a ship: Underwater Noise and Hydrodynamic Performance

Chengyi Zhou[a], Danlei Yang[a, b, *], Blanca Pena[a], Tim Wood[c], Luofeng Huang[a, *]

[a]Faculty of Engineering and Applied Sciences, Cranfield University, Cranfield, MK43 0AL, United Kingdom

[b]Department of Engineering, City St George's University of London, London, EC1V 0HB, United Kingdom

[c]Achelous Energy Limited, Unit 2 Black Robins Farm, Edenbridge TN8 6QP, United Kingdom

Corresponding authors: danlei.yang@citystgeorges.ac.uk (D.Yang); luofeng.huang@cranfield.ac.uk (L. Huang)

Abstract

Hydrofoils installed upstream of a ship propeller offer opportunities to alter underwater noise and ship hydrodynamics, but this has rarely been proven in experiments and the underlying mechanisms remain unclear. This study experimentally investigates hydrofoils, inspired by whales' tubercled flippers, mounted ahead of the propeller of a KVLCC2-type model tanker. Thirty configurations, varying mounting position, wingspan, chord length and tubercle number, were evaluated over 147 runs against a bare-hull reference. Underwater pressure spectra were analysed at 13 selected frequency bands, and vessel advance performance was characterised by distance per revolution (DPR). Across the tested configurations, the largest observed reduction in sound pressure spectral density level at an individual target frequency was 7.03 dB, corresponding to approximately an 80.2% reduction in pressure power spectral density at that frequency, while the highest configuration-mean DPR reached 22.03 mm/rev, representing a 7.8% increase over the bare-hull reference. These maxima represent separate acoustic and advance-performance outcomes rather than a simultaneous improvement by one configuration. Many configurations also increased spectral levels or reduced DPR, and no configuration demonstrated a consistent advantage across both performance measures and all selected

frequency bands. Tubercle effects were strongly geometry-dependent: adding five tubercles to hydrofoils with a 40 mm wingspan lowered the mean spectral level by 1.85 dB at a 20 mm chord but raised it by 1.17 dB at a 40 mm chord relative to the corresponding smooth hydrofoils. These findings prove the potential benefits of this application for noise control and hydrodynamic enhancement, motivating further investigations into the physics.

Keywords: Hydrofoil, Underwater noise, hydroacoustics, hydrodynamics, experiments.

Nomenclature

A	amplitude (peak-to-trough distance)
λ	wavelength
C	chord length
W	wingspan length
N	number of tubercles
P	position of hydrofoil
LET	Leading-edge tubercle
DPR	distance per revolution
L_p	sound pressure spectral density level
CV	coefficient of variation
Fr	Froude number
Re	Reynolds number
U	vessel advance velocity
X_0	chordwise coordinate on the original hydrofoil profile
X_{mod}	chordwise coordinate on the modified peak profile
f	frequency
G_f	sound pressure power spectral density at frequency f (μPa²/Hz)
p_{ref}	reference sound pressure (1 μPa)
μ	mean of repeated measurements
σ	standard deviation of repeated measurements
SS	sum of squares
$SS_{between}$	between-group sum of squares
SS_{within}	within-group sum of squares
F	ANOVA F-statistic
p	statistical p-value
k	number of factor levels in the one-way ANOVA

g	group index in the one-way ANOVA
n	total sample size used in the analysis
n_g	number of observations in group g
y_{gi}	observation i in group g
$\bar{y}_g$	mean response in group g
$\bar{y}$	overall mean response
d	target design parameter in the net effect analysis
i, j	configuration index and adjustment-factor index, respectively
$\mathcal{C}$	set of the three non-target design parameters used for adjustment
y_i	response of configuration i
$x_{i,j}$	level of parameter j for configuration i
$1[x_{i,j}]$	indicator (dummy) variables for the levels of parameter j
β_0	regression intercept
β_j	regression coefficients for parameter j
e_i	regression residual for configuration i
ℓ	level of the target design parameter
d_i	level of the target parameter for configuration i
n_ℓ	number of configurations at level ℓ
$\bar{e}_\ell$	mean residual at level ℓ (estimated net effect)
s^2_ℓ	sample variance of residuals at level ℓ
ℓ_a, ℓ_b	two factor levels compared in the t-test
t	two-sample t-statistic
ANOVA	analysis of variance
AOA	angle of attack
CAD	computer-aided design
CFD	computational fluid dynamics
IMO	International Maritime Organization
ITTC	International Towing Tank Conference
PLA	polylactic acid
RPS	propeller rotational speed in revolutions per second
SD	standard deviation
STFT	short-time Fourier transform
NoBlade	static test with a blade-less dummy propeller
RegularSt	static test with the regular propeller
RegularDy	dynamic test with the regular propeller

1. Introduction

Global shipping requires the use of large cargo vessels or oil tankers to travel long distances. Massive amounts of energy are consumed during this process, with significant greenhouse gas emissions. Underwater radiated noise from shipping, generated by propeller cavitation, machinery vibration and hull-induced flow noise, has also been linked to adverse impacts on marine life [1]. The International Maritime Organisation (IMO) proposed a net-zero carbon emission goal in 2050 [2] and highlighted guidelines for lowering underwater noise [1,3]. Humpback whales are large marine animals whose tubercled flippers, shown in Figure 1, have been shown to reduce drag and delay stall [4]. Research has been conducted on this tubercled feature using computational fluid dynamics (CFD) simulations and experiments over time.



Figure 1. Humpback whales' tubercled flippers (Source: Wikimedia Commons, under CC BY license) [5]

Treating the whales' tubercled flipper as an isolated structure, it is usually referred to as a leading-edge tubercle (LET) aerofoil or hydrofoil. Simulations of the LET hydrofoil have mainly focused on its dynamic performance and underlying mechanism. Tested in airflows, Watts and Fish [6] first showed a 4.8% rise in lift and a 10.9% reduction in drag using a tubercled wing at a 10° angle of attack (AOA). Fan et al. [7] confirmed this mechanism at a higher Reynolds number ($Re = 5\times10^5$) using the NACA 4415 aerofoil as a baseline: two LET aerofoils were created, one with both peak and trough sections, another with only the peak section, and both generated counter-rotating vortex pairs that enhanced the lift-drag performance in the post-stall region at high AOA. The peak-only construction resulted in better aerodynamic characteristics. Consistent with the role of these vortex pairs, Wei et al. [8] conducted experiments in a water tunnel at a very low Reynolds number ($Re = 1.4\times10^4$) and identified a trade-off: hydrofoils with a larger amplitude-to-wavelength (A/λ) ratio show less flow separation but become more unstable in time, especially at high AOA [9]. Further experiments extended this trade-off to finite-span wings rather than end-plated hydrofoils at $Re = 1.8\times10^5$ [10], highlighting the importance of the ratio between tubercle amplitude and chord length, and between wavelength and chord length; the wing-tip vortex was found to partially reduce the tubercles' effect, but was not the dominant factor. Taken together, these studies show that LETs consistently improve stall and post-stall performance, but the size and even the sign of this benefit depend strongly on tubercle geometry and operating condition.

However, most research on tubercled wings has focused on lift-drag performance, and acoustic characteristics have rarely been studied. Among the few studies of noise, Kimmerl and Abdel-Maksoud [11] visualised the underwater noise field using statistical moments of pressure in simulations, without tubercled geometry. Closer to a design context, Knox et al. [12] identified a Pareto-optimal front between noise and propeller efficiency across a range of propeller designs, showing that reducing one often comes at the cost of the other. In an experimental setting, Tani et al. [13] developed a wire-based measurement system in a towing tank to capture propeller wake and noise level, following International Towing Tank Conference (ITTC) guidance [14], and observed and photographed the formation of cavitation. None of these studies, however, considered a LET hydrofoil, so how the geometry-dependent trade-offs identified above translate into acoustic behaviour remains unknown.

Applications of the LET structure have extended beyond isolated hydrofoils to propulsion components. Stark et al. [15] applied LETs to a ducted propeller and found that the tubercle structure enhanced duct thrust capability but decreased propeller thrust and torque, with the penalty worsening at greater advance ratio. Fan et al. [7] similarly found, on blades, that the peak-only tubercle construction resulted in better thrust performance across a range of propeller rotational speeds, in agreement with their own hydrofoil findings. Shi et al. [16] tested a NREL S814 propeller with different numbers of tubercles at the blade tip and found that, at low tip speed ratios up to 2.5, the tubercled propeller enhanced both torque and thrust in stall conditions. Alongside these propeller-focused studies, improvements in vessel performance have typically been pursued by optimising vessel geometry [17,18] or altering bulbous bow size [19]; the application of LET structures in this context remains scarce.

Overall, previous studies agree that LETs improve hydrodynamic performance in the stall and post-stall regime and can enhance propulsive thrust when applied to propellers and turbines, but their acoustic consequences have received far less attention, and studies that directly couple LET geometry, underwater noise and the performance of a model vessel remain limited. This study therefore investigates experimentally how a LET hydrofoil installed ahead of the propeller of a model tanker affects underwater noise and vessel performance, and which design parameter dominates these effects. Hydrofoils with different chord lengths, wingspans and numbers of tubercles were mounted at three positions ahead of the propeller of a KVLCC2 model (30 configurations in total) and tested while the model advanced freely in a towing tank. Underwater noise was recorded by a hydrophone and expressed as sound pressure level, while vessel performance was evaluated from advance velocity and distance per revolution measured by stereo cameras. The results were analysed using CV, ANOVA and net effect analysis to identify the dominant parameter and the direction and magnitude of its effect. The present study focuses on the relative comparison between hydrofoil configurations at model scale; scaling of the acoustic results to full-scale vessels is beyond the present scope. The findings provide an experimental basis for LET design on vessels where underwater noise and propulsion performance must be considered together.

The remainder of this paper is organised as follows. Section 2 describes the design and manufacture of the LET hydrofoils. Section 3 presents the experimental setup, including the towing tank, model vessel and test procedure. Section 4 explains the data processing and the statistical analysis methods. Section 5 presents and discusses the results, and Section 6 concludes the study.

2. Design of Hydrofoils

The baseline hydrofoil was based on the NACA 4420 profile. It is thicker than the NACA 4415 profile used in earlier LET studies [7], and the extra thickness provided room for mounting hydrofoils on the bottom surface of the vessel. Four design parameters were varied (Table 1): the position ahead of the propeller (P), the wingspan (W), the chord length (C) and the number of tubercles (N). Two wingspans (W = 20 and 40 mm) and two chord lengths (C = 20 and 40 mm) were combined, which gave span-to-chord ratios of W/C = 0.5, 1 and 2. These dimensions kept the hydrofoil within the projection of the vessel's outer boundary, so that it was not damaged during docking. Three tubercle numbers were used (N = 0, 5 and 10), where N = 0 denotes a smooth hydrofoil without tubercles, which served as the control for each W–C combination. An example is shown in Figure 2.

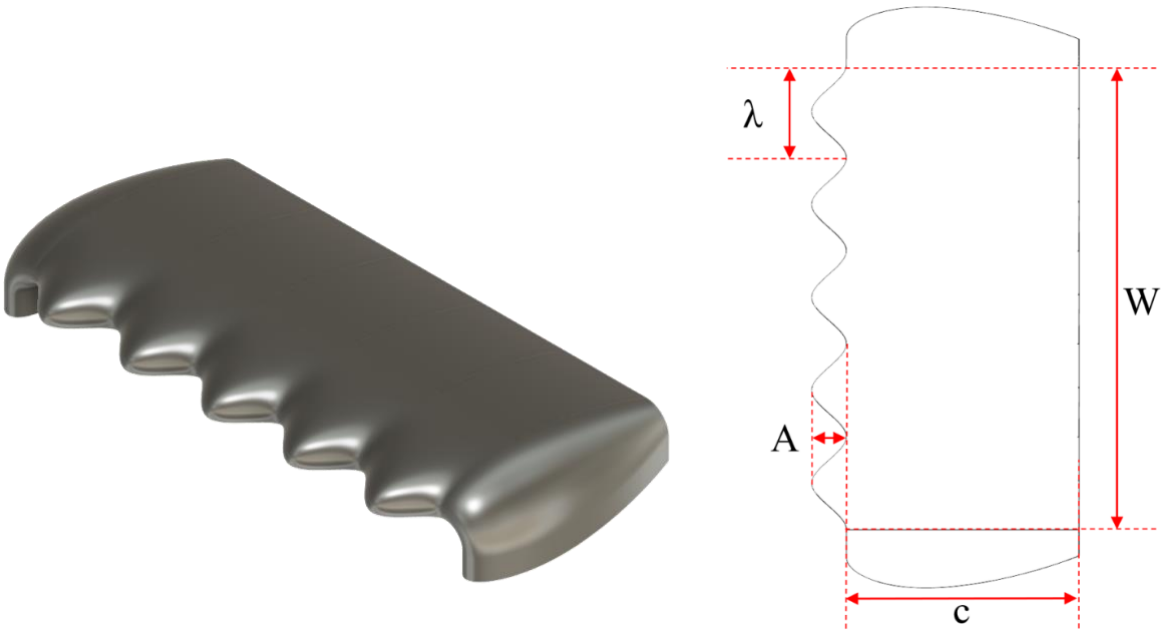


Figure 2. The geometric parameter labelled on a LET hydrofoil

The tubercle amplitude A, defined as the peak-to-trough distance, was fixed at 3 mm, which gives A/C = 0.15 for C = 20 mm and 0.075 for C = 40 mm. The value A/C = 0.1 used by Fan et al. [7] lies between the two. The tubercles were evenly spaced along the span with a wavelength λ = W/N, so that the amplitude-to-wavelength ratio A/λ = 3N/W was 0.375, 0.75

or 1.5, depending on W and N. Because A is a peak-to-trough distance, A/λ here is twice the value obtained when A is defined as the sinusoidal amplitude, as in Wei et al. [8].

The tubercled hydrofoil was built from two profiles: the original NACA 4420 profile, used as the trough profile, and a modified peak profile. Following the peak-and-original-section construction of Fan et al. [7], the peak profile was obtained by shifting the points of the original profile forward with a smooth chordwise function of equation (1).

$$X_{mod}(x) = X_0(x) - \frac{A}{2}\left[1 + cos\left(\frac{\pi X_0(x)}{0.3C}\right)\right] \quad 0 \le X_0(x) \le 0.3C \qquad \textbf{(1)}$$

where X_0 is the chordwise coordinate of a point on the original profile, measured from the leading edge (X_0= 0) towards the trailing edge (X_0 = C), X_{mod} is the coordinate of the same point on the peak profile, A is the amplitude and C is the chord length of the original profile. Points behind X_0 = 0.3C were not shifted. The shift equals A at the leading edge, so the peak profile has a chord of C + A. The shift and its slope both vanish at X_0 = 0.3C, the position of maximum thickness, so the modified region blends smoothly into the unchanged aft section, showing in Figure 3. The peak and trough profiles were placed alternately at intervals of λ/2 along the span, with a trough section at each end, and joined with the "Loft" function of the CAD software to form a smooth leading-edge waveform with N peaks. The hydrofoils were manufactured by 3D printing in PLA.

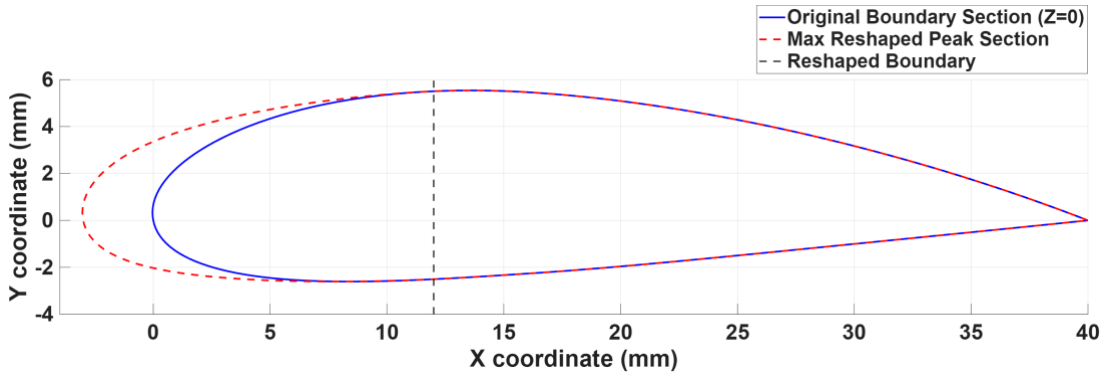


Figure 3. Peak and original cross-section profile of a LET hydrofoil

The four factors define a full factorial of 3 × 2 × 2 × 3 = 36 combinations. Thirty of them were tested, numbered C2–C31 (Table 1), together with a reference case without a hydrofoil (C1). The six combinations not included in the present test campaign are the 20 mm × 20 mm hydrofoils with 5 and 10 tubercles at each of the three positions due to time limitation. The design is therefore an incomplete factorial: the smooth hydrofoil (N = 0) was tested at all four

span–chord combinations and serves as the matched control, whereas N = 5 and 10 were tested at three of the four combinations. The consequence for the statistical analysis is described in Section 4.

Table 1. The parameters detail for each hydrofoil testing case. C1 is the reference case without a hydrofoil. N = 0 denotes a smooth hydrofoil

Label	Position (mm)	Wingspan (mm)	Chord length (mm)	Number of tubercles
C1	None	None	None	None
C2	30	40	40	0
C3	100	40	40	0
C4	170	40	40	0
C5	30	40	40	5
C6	100	40	40	5
C7	170	40	40	5
C8	30	40	40	10
C9	100	40	40	10
C10	170	40	40	10
C11	30	40	20	0
C12	100	40	20	0
C13	170	40	20	0
C14	30	40	20	5
C15	100	40	20	5
C16	170	40	20	5
C17	30	40	20	10
C18	100	40	20	10
C19	170	40	20	10
C20	30	20	40	0
C21	100	20	40	0
C22	170	20	40	0
C23	30	20	40	5
C24	100	20	40	5
C25	170	20	40	5
C26	30	20	40	10
C27	100	20	40	10
C28	170	20	40	10
C29	30	20	20	0
C30	100	20	20	0
C31	170	20	20	0

3. Experimental Setup

3.1 Towing Tank Facility and Model Vessel

The experiments were performed in a towing tank with a total length of 30 m, width of 1.9 m and water depth of 1.5 m, shown in Figure 4. The testing area is 7.5 m in length, located at the tank centre. Two stereo cameras were mounted 1.7 m above the water level, measuring vessel velocity, as explained in Section 4.2. Two wooden frames formed a railway system, constraining the aluminium mast, forcing the vessel to advance in a straight path. The testing model vessel is similar to a KVLCC2 tanker, an open-source hull form validated by multiple experimental and CFD studies [20]. The hull was 3D-printed in PLA at a 1:191 scale of length, shown in Figure 4. Particulars of the model and full-scale vessel are given in Table 2. A test velocity U = 0.216 m/s was chosen, resulting in a Froude number of Fr=0.0533. The hydrofoils were mounted at P = 30, 100 and 170 mm ahead of the propeller blade section.

Table 2. Particulars of the model vessel and KVLCC2 tanker [21,22]

	Model	KVLCC2
Length of Hull (m)	1.675	320.0
Maximum Breadth (m)	0.3036	58.0
Depth (m)	0.157	30.0
Draught (m)	0.109	20.8
Test Velocity (m/s)	0.216	2.986
Froude Number	0.0533	0.0533

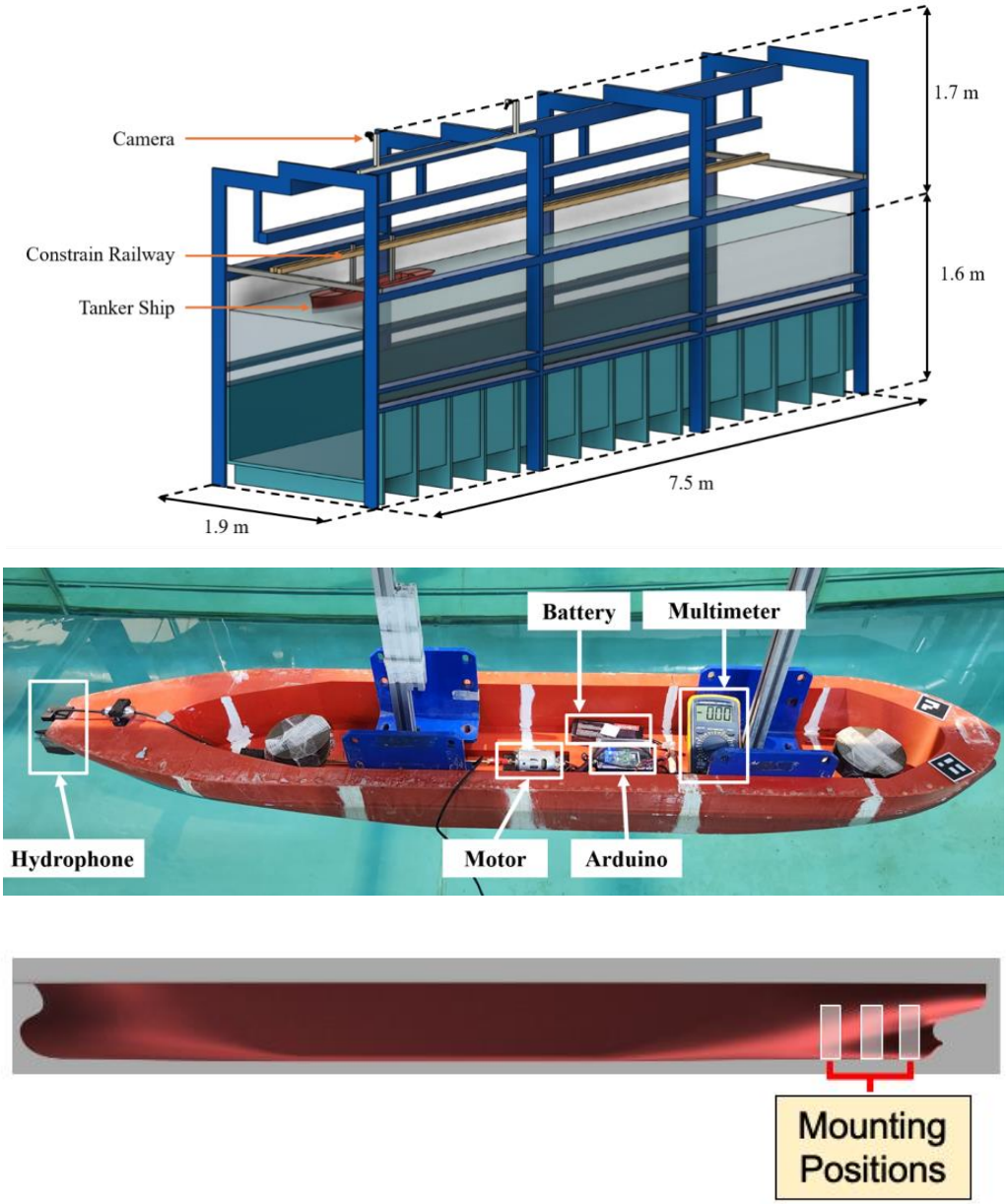


Figure 4. The towing tank (Top) and the testing model vessel (Bottom)

3.2 Test Series

Five repeated tests were performed for each hydrofoil configuration, and the 31 configurations were tested in order listed in Table 1. Approximately one minute was allowed between successive runs to let the water surface settle. Water temperature was not measured during testing. The battery supplying the propeller motor was recharged or replaced for each 9 configurations, as this would affect the propeller rotational speed within each set. To remove

this dependency, the distance per revolution (DPR) rather than the absolute rotational speed or advance velocity was used to characterise vessel performance (Section 4.2).

1) The underwater background noise was first quantified for the testing environment to determine its significance. All devices remained turned off while the ship was stationary. The background noise was considered negligible if it is more than 10 dB below the noise level recorded during subsequent testing.
2) Blade-generated noise was isolated from mechanical and electrical vibration by comparing two propeller conditions: a blade-less dummy propeller and a regular propeller, both rotated at a matched speed of approximately 9.25–11.4 revolutions per second while the vessel remained stationary. This procedure followed ITTC guidance [14].
3) A reference dynamic test provided baseline noise and velocity data for comparison with the hydrofoil results. The vessel travelled freely along the towing rail without a hydrofoil installed, using the same regular propeller described above.
4) Finally, all 30 hydrofoil configurations listed in Table 1 were tested dynamically under the same conditions as the reference case, with the hydrofoil mounted upstream of the propeller at the position, wingspan, chord length, and tubercle number specified for each configuration.

4. Data Processing and Statistical Analysis

4.1 Noise Data and Sound Pressure Spectral Density Level

The propeller-induced noise was measured using and Aquarian Scientific AS-1 hydrophone, connected to an AMS-22 amplifier. The acoustic centre was defined at the propeller centre, with the hydrophone positioned 35 mm downstream of this reference point, shown in Figure 5. The signal was sampled at 44.1 kHz.

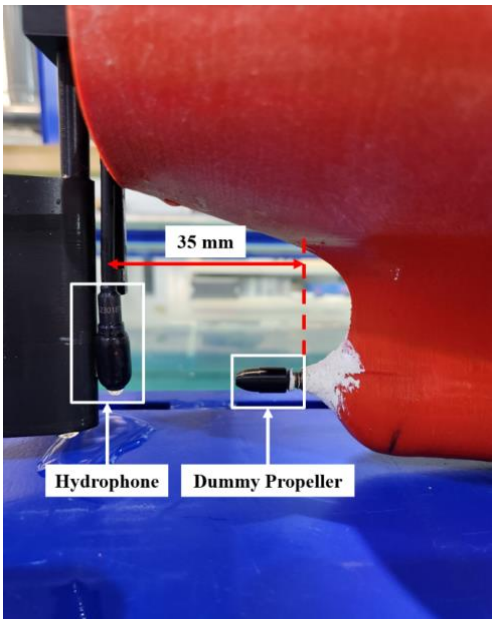


Figure 5. The hydrophone position demonstrated using a no-blade dummy propeller

The average power spectral density $G(f)$, in units of μPa²/Hz, was estimated from each sound pressure signal using Welch's method with Hann window. The resulting sound pressure spectral density level (L_p) is calculated as:

$$L_p = 10\,log_{10}\left(\frac{G(f)}{{p_{ref}}^2}\right) \quad \textbf{(2)}$$

where p_{ref} = 1 μPa and L_p is in unit of dB re 1μPa²/Hz [13,14].

Prior to computing the final L_p spectrum, the raw signal was processed using a Short-Time Fourier Transform (STFT) to check for interference, as shown in Figure 6. The resulting spectrogram was visually inspected to identify interference-free segments initially; a sudden colour change indicated an abrupt shift in the noise signature. Data recorded beyond this point were therefore excluded from analysis. All data were processed within a minimum 20 second window where the ship speed is stable, following ITTC guidance [13,14] . The position of this window was selected among the four or five repeat measurements of each configuration. The target frequencies were identified by the spectrum peak after Fourier transform. Throughout data collection, the recorded voltage remained within the amplifier's full-scale range, confirming that no signal clipping or distortion occurred.

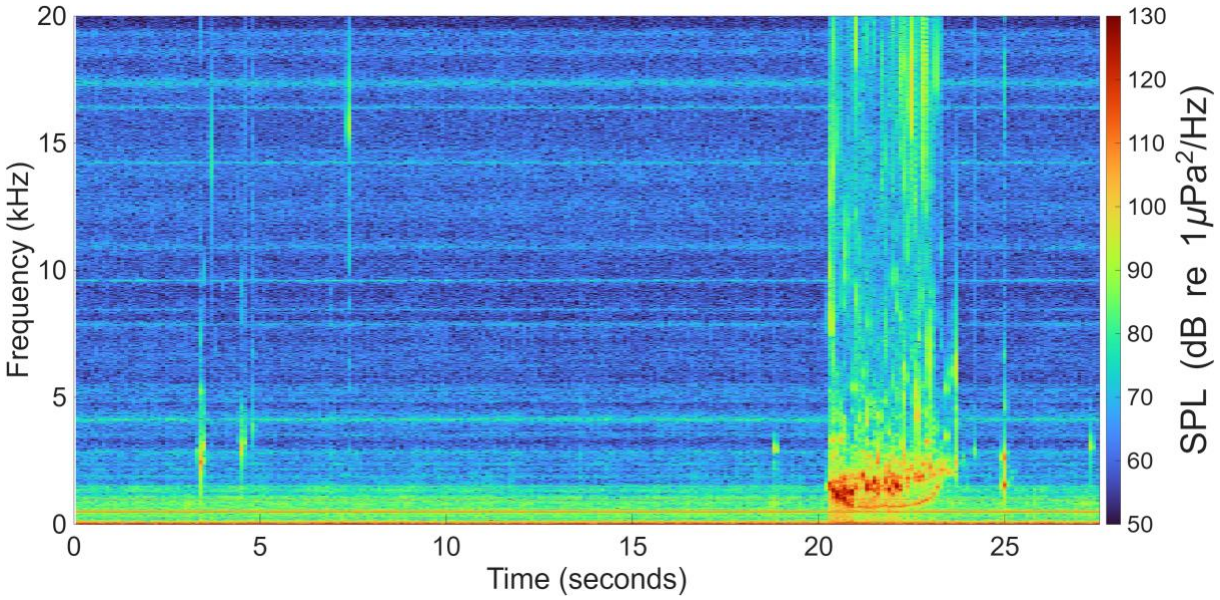


Figure 6. The Short-Time Fourier Transform

4.2 Velocity and Distance per Revolution

Two identical cameras (DAHeng Imaging MER3-1610-52U3DM) with frame of 20 fps, were mounted 1.7 m above the towing tank, approximately 2 meters apart, with their fields of view overlapping to cover the 1 m test section.

Three position markers (P1, P2, P3) were placed at equal intervals of 0.5 m over the 1 m terminal test section, representing the start, mid-way and end points respectively (Figure 7). As the vessel passed each marker, the corresponding stereo image pair was recorded together with its frame number and timestamp. The vessel velocity over each half-section (P1–P2 and P2–P3) was calculated as the marker spacing divided by the elapsed time between the corresponding frames, and the two half-section velocities were compared to verify that the vessel had reached a steady speed within the test section. The mean of the two segment velocities was then used as the representative vessel velocity for each run.

The vessel's motor was powered by a 7.4 V lithium battery under 1 V. The voltage output of which dropped with continued use, reducing the propeller rotational speed and vessel speed. Because this drop affected the motor and the resulting thrust in a broadly proportional manner, the ratio between vessel speed and propeller rotational speed, which is the distance per revolution (DPR, equation (3)), was expected to remain largely insensitive to this effect. The propeller rotational speed was determined by the corresponding frequency of the maximum L_p

peak, and DPR was therefore used, alongside the camera-derived velocity, to characterise vessel performance.

$$DPR = \frac{U}{RPS} \tag{3}$$

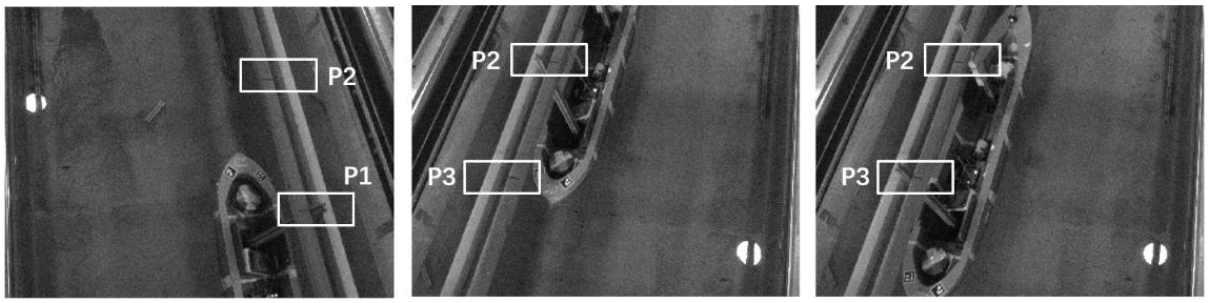


Figure 7. Stereo camera image capturing vessel movement, with position markers P1, P2, and P3 highlighted

4.3 Statistical Analysis Framework

After completing experiments, four or five data for the 30 configurations (excluding C1 with no hydrofoil), including sound pressure level and distance per revolution were carried into three statistical methods by sequence: Coefficient of Variation (CV), Analysis of Variance (ANOVA) and Net Effect Analysis.

The Coefficient of Variation (CV) was used to assess the repeatability of each test configuration, calculated as equation (4), where μ and σ are the mean and standard deviation of the four or five repeated runs for a given quantity of vessel velocity, DPR, or L_p.

$$CV = \frac{\sigma}{\mu} \tag{4}$$

The Analysis of Variance (ANOVA) is a statistical method used to determine whether changing a parameter produces a significant difference in the response, by comparing the variation between groups to the variation within each group. One-way ANOVA was applied separately to each of the four design parameters: position (P), wingspan (W), chord length (C) and number of tubercles (N). Equation (5) and (6) show the sum of squares SS between and within group. k is the number of levels of the parameter (e.g. 3 for tubercles number N as N=0, 5 and 10); g indexes the groups from 1 to k, and n is the total sample size; $\bar{y}_g$ is the group mean; and $\bar{y}$ is the overall mean. F is the ratio of the two mean squares. Equation (7) uses F to indicate whether

a parameter has substantial effect, while the effect is negligible if $F < 1$. The p value in equation (8) is a probability between 0 and 1. A p-value below 0.05 was taken to indicate that the parameter has a statistically significant effect on the response. For each response variable, DPR, and L_p found to be significant were carried forward to the net effect analysis with all four design parameters.

$$SS_{between} = \sum_{g=1}^{k} n_g \left(\bar{y}_g - \bar{y}\right)^2 \quad \textbf{(5)}$$

$$SS_{within} = \sum_{g=1}^{k} \sum_{i=1}^{n_g} \left(y_{gi} - \bar{y}_g\right)^2 \quad \textbf{(6)}$$

$$F = \frac{SS_{between}/(k-1)}{SS_{within}/(n-k)} \quad \textbf{(7)}$$

$$p = P\left(F_{k-1,n-k} \geq F\right) \quad \textbf{(8)}$$

A net effect analysis was used to quantify the direction and magnitude of the change in the response caused by each parameter after the influence of the other three parameters had been removed.

For a target parameter d, the response of the 30-configuration means was first regressed by ordinary least squares on the other three parameters, each treated as a categorical variable using equation (9) [23]. y_i is the response (the L_p in dB or the DPR in mm/rev) of configuration i, $\mathcal{C}$ is the set of the other three parameters, $\mathbb{1}[x_{i,j}]$ are the indicator (dummy) variables for the levels of parameter j (excluding its reference level), β_0 is the intercept, β_j are the regression coefficients, and e_i is the residual, which contains the effect of d together with random error.

$$y_i = \beta_0 + \sum_{j \in \mathcal{C}} \beta_j \ \mathbb{1}[x_{i,j}] + e_i \quad \textbf{(9)}$$

The net effect of level ℓ of parameter d was defined as the mean residual of the configurations at that level using equation (10). n_ℓ is the number of configurations at level ℓ. A positive (negative) $\bar{e}_\ell$ means that the response at this level was higher (lower) than expected from the other three parameters, and the difference between two levels gives the size of the effect of changing d, in the unit of the response. The difference between two levels ℓ_a and ℓ_b was tested

with a two-sample t-test on the residuals, using equation (11), and $p < 0.05$ was taken as significant.

where $s^2{}_\ell$ is the sample variance of the residuals at level ℓ. The parameters with two levels (W and C) gave one comparison each, and those with three levels (P and N) gave three.

$$\bar{e}_\ell = \frac{1}{n_\ell} \sum_{i:\, d_i = \ell} e_i \tag{10}$$

$$t = \frac{\bar{e}_{\ell_b} - \bar{e}_{\ell_a}}{\sqrt{s^2_{\ell_a}/n_{\ell_a} + s^2_{\ell_b}/n_{\ell_b}}} \tag{11}$$

The analysis was applied to the seven target frequencies at which the ANOVA found at least one significant parameter, and to all four parameters at each of them, which gave 56 comparisons. Net effect analysis adjusts for the other parameters assuming that their effects are additive, so interactions between parameters could not be assessed. Because the design is unbalanced, the residual-based estimate is slightly smaller in magnitude than the coefficient of a model containing all four parameters, so it is conservative. The comparisons were not corrected for multiple testing; at the 0.05 level about 2.8 (56 × 0.05) significant results are expected by chance, which is considered in the interpretation (Section 5).

5. Results and Discussion

5.1 Noise Sources and Target Frequencies

The L_p spectra from 0 to 50 Hz of the four baseline conditions are compared in Figure 8, computed with 2000 ms windows, a frequency resolution of 0.5 Hz. The background spectrum is nearly flat, between 75 and 85 dB re 1 µPa²/Hz. With the motor powering a no-blade propeller (NoBlade), the spectrum peaks appear at approximately 13, 26.5 and 39.5 Hz, corresponding to the shaft rotation frequency and its second and third harmonics. These peaks reach about 120 dB, while the broadband level between them remains close to the background. With the regular three-blade propeller fitted in the static test (RegularSt), the same series appears at approximately 10.5, 21 and 31.5 Hz. As the voltage input was the same, the lower shaft frequency is probably caused by the additional hydrodynamic load of the propeller. For this three-bladed propeller, the blade-passing frequency (3 × 10.5 Hz ≈ 31.5 Hz) coincides with the third shaft harmonic. The dynamic test (RegularDy) shows the same harmonic series, with the

whole spectrum 5 to 12 dB higher. Possible causes are effects that are present only when the vessel is moving, such as non-uniform inflow from the hull wake and hydrodynamic pressure fluctuations, but the present data cannot separate their contributions.

The peak near 21 Hz requires particular care. The observations are as follows. In RegularSt, the peak at 21 Hz coincides with the second harmonic of the 10.5 Hz shaft frequency (2 × 10.5 = 21 Hz). However, the NoBlade spectrum also contains a tonal peak at about 21 Hz (about 119 dB), which is not a harmonic of its own 13 Hz shaft frequency, since the second harmonic of 13 Hz is the 26.5 Hz peak. The STFT shows that this component is present throughout the NoBlade recording, as persistently as the 13 Hz component. In the additional static tests at 1800 and 4300 mV, the motor rotated faster, giving shaft frequencies of approximately 15 and 19.5 Hz and spectrum levels 20–23 dB higher than the regular static test at 1000 mV, and no peak appears at 21 Hz (Figure 8). A fixed-frequency source would remain at 21 Hz regardless of rotation speed, so the absence of the peak at higher voltages suggests that the 21 Hz peak in RegularSt is the second shaft harmonic rather than a fixed-frequency motor tone. This is not conclusive: a weak fixed tone could be masked by the higher broadband level at these voltages, and in RegularSt a shaft harmonic and a fixed tone would fall at the same frequency and cannot be separated. The origin of the 21 Hz tone in the NoBlade condition remains unresolved.

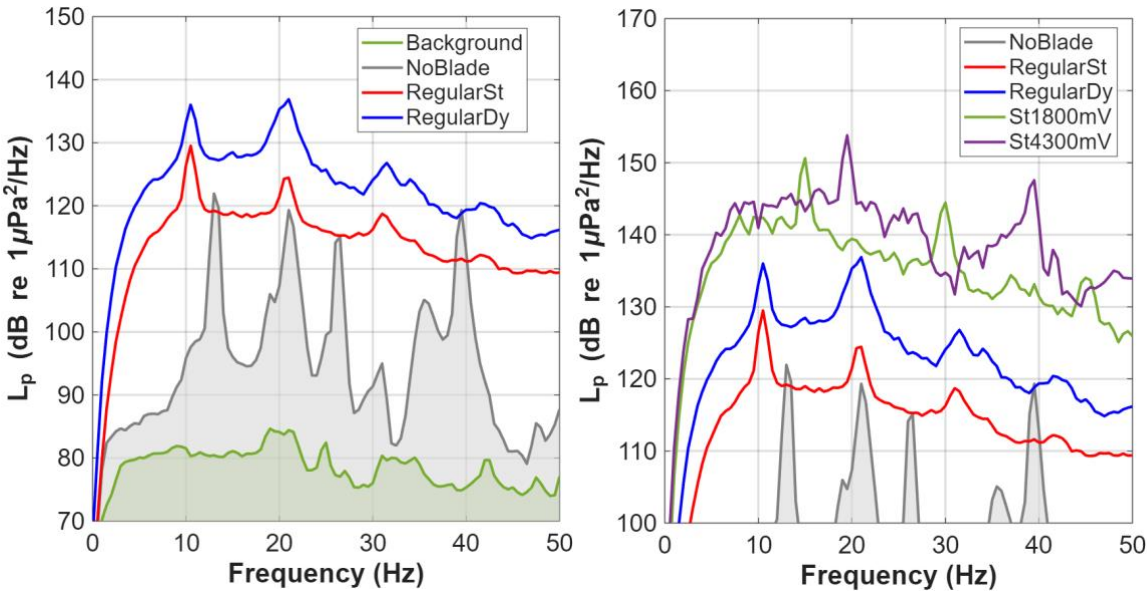


Figure 8. The L_p for shaft and propeller frequencies at baseline conditions (Left) and static test with greater voltage input (Right)

The result of L_p at higher frequency is shown in Figure 9, using 50 ms windows and frequency resolution of 20 Hz. Background noise was at least 12 dB lower than all other conditions, confirming it did not confound the results. In both the static and dynamic tests, spectral peaks appear at 500, 1000, 4120, 7880, 8440, 9580, 10860, 14200, 16420, 17360, 18580 and 19340 Hz. These frequencies were selected as the target frequencies for the hydrofoil analysis because first, they are narrow-band components that stand out above the broadband spectrum; and second, they were present in both the static and the dynamic tests, the latter being the condition of the hydrofoil tests; and last, they cover the range from 500 to 19340 Hz. The 20 Hz band was added because, with the 20 Hz resolution, it contains the shaft frequency and its second harmonic. When the voltage input was increased to 1800 and 4300 mV (Figure 10), the target frequencies did not shift. They are therefore not harmonics of the shaft rotation.

Particular attention was paid to 500 and 19340 Hz, where peaks of similar width appear in both the NoBlade and the regular-propeller conditions, showing in Figure 10, so these peaks are not generated by the blades. The 500 Hz peak is absent from the background recording, which indicates that it comes from the powered motor or other equipment; this could be tested by measuring at the minimum voltage before the motor starts rotating. The 19340 Hz peak is close to the Nyquist frequency of the recording, 22.05 kHz for a 44.1 kHz sampling rate, so it may be an artefact, which could be checked with a higher sampling rate such as 96 kHz. The L_p at 20, 500 and 19340 Hz is therefore interpreted with caution in the analysis of the hydrofoil effects.

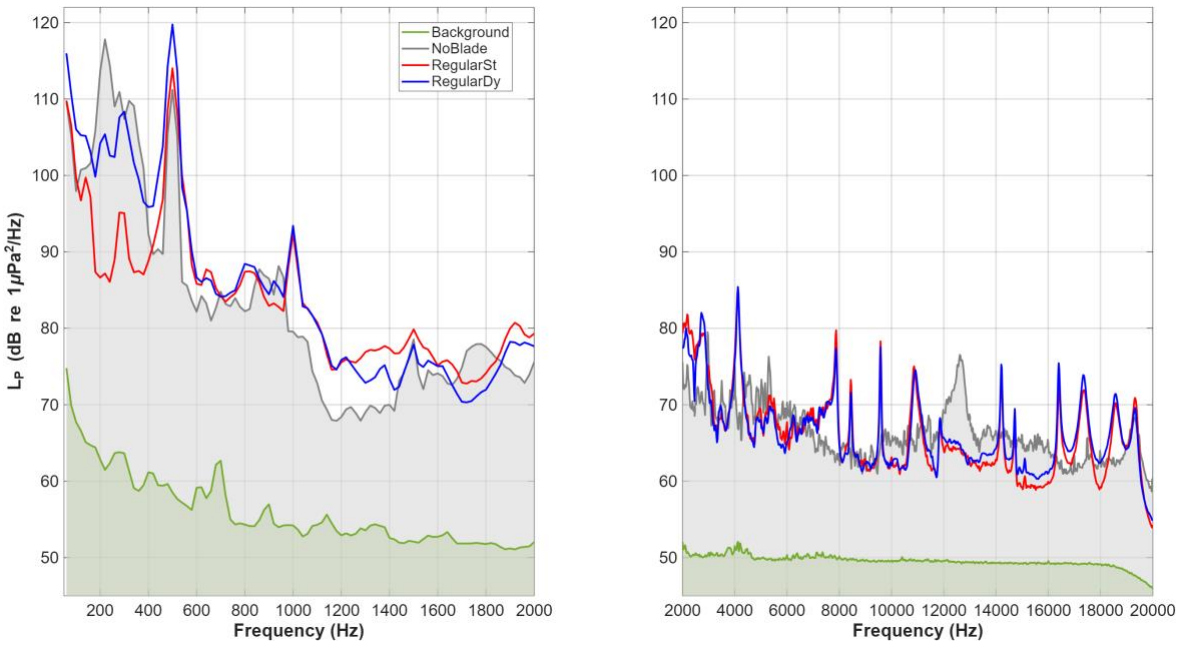


Figure 9. The L_p for different test series between 50 Hz and 20000 Hz

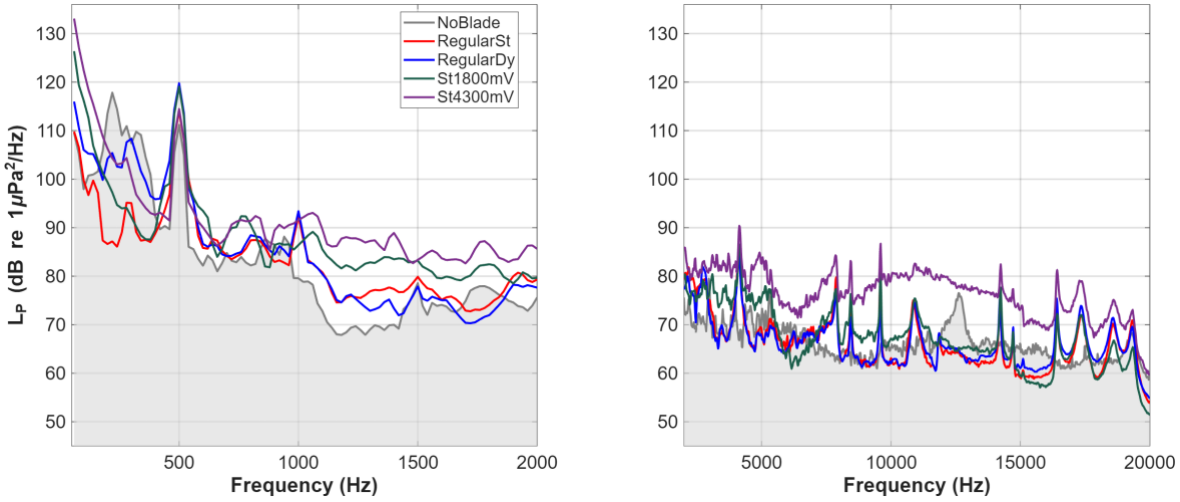


Figure 10. The L_p with greater voltage input

5.2 Hydrofoil and Bare Hull Performance

Experiments were performed with the 30 hydrofoil configurations and the bare hull reference conditions. The L_p and DPR of each run are plotted in Figure 11, and the CV of the four or five repeats of each hydrofoil configuration is shown in Figure 12.

The comparison reference was the bare hull tested on different days. The bare hull results varied between runs. The DPR averaged 20.44 mm/rev with SD = 1.08 mm/rev. 73.3% fell within ±1.0 mm/rev. For L_p, averaged over the 13 frequency bands, 80% of the runs fell within ±2 dB and 94.4% within ±3 dB of the mean, although the share at ±3 dB varied from 80–86.7% at 4120, 7880 and 10860 Hz to 100% at 9580, 14200 and 18580 Hz. When both criteria were applied together, 71.8% of the bare hull runs lay inside a window of ±3 dB and ±1.5 mm/rev. The causes of the variation were not identified; possible causes are changes in the vessel launching conditions, the water temperature and residual water motion in the tank.

Across the 30 hydrofoil configurations with a total of 147 runs, the mean velocity was 220.9 mm/s, the mean RPS was 10.69 Hz and the mean DPR was 20.67 mm/rev, which were close to the bare hull values of 216.09 mm/s, 10.56 Hz and 20.44 mm/rev. The configuration-mean DPR ranged from 18.40 to 22.03 mm/rev, corresponding to a deviation of −2.04 to +1.59 mm/rev from the bare hull mean. Nine of the 30 hydrofoils exceeded the bare hull DPR by more than 1 mm/rev, 17 fell within ±1 mm/rev, and the other 4 were lower by more than 1 mm/rev.

For L_p, the configuration-mean level averaged over the 13 bands was 0.71 dB higher than the bare hull and ranged from −1.07 to +3.17 dB, and 13 of the 30 configurations were more than 1 dB higher. The offset depended on the frequency. It was largest at 14200 Hz at +3.19 dB, 16420 Hz at +2.30 dB and 17360 Hz at +2.02 dB, whereas the levels at 4120 Hz, 20 Hz and 500 Hz were slightly lower than those of the bare hull, by 0.57, 0.27 and 0.23 dB, respectively. On average, 83.3% of the band-level differences between a configuration and the bare hull were within ±3 dB, and only three configurations had all 13 bands within ±3 dB. The levels exceeded the bare hull by more than 3 dB for 19 configurations at 14200 Hz, 8 at 17360 Hz, 6 at 16420 Hz and 5 at 1000 Hz. Levels fell more than 3 dB below the bare hull for 11 band–configuration combinations, at 20, 500, 1000, 10860 and 19340 Hz, with the lowest difference of −7.03 dB.

No configuration was clearly quieter than the bare hull. The lowest mean offset was −1.07 dB for P100W40C40N0, which was smaller than the bare hull SD of 1.71 dB. The three quietest configurations were P100W40C40N0 at −1.07 dB, P30W40C20N5 at −0.83 dB and

P170W40C40N0 at −0.73 dB. They were lower than the bare hull in 9, 8 and 8 of the 13 bands, respectively, and all had W = 40 mm. Among them, P170W40C40N0, a smooth hydrofoil, also had a high DPR of 21.98 mm/rev, which was 1.54 mm/rev above the bare hull. It was the only configuration with a lower L_p, and a DPR increase of more than 1 mm/rev, so it was the best compromise between noise and DPR. The effect of tubercles depended on the chord length. For W = 40 mm and C = 20 mm, tubercles lowered the mean L_p, offset from +1.30 dB without tubercles to −0.55 dB with N = 5 and −0.16 dB with N = 10, whereas for C = 40 mm they raised it from −0.53 dB without tubercles to +0.64 dB with N = 5 and +2.59 dB with N = 10. For W = 20 mm and C = 40 mm, tubercles had little effect, with offsets of +1.01, +1.04 and +1.11 dB for N = 0, 5 and 10. The four loudest configurations had offsets of +2.17 to +3.17 dB, and all had W = 40 mm, C = 40 mm and N = 5 or 10. Their largest excess was at 16420 Hz at +5.2 dB, 14200 Hz at +4.8 dB and 17360 Hz at +4.0 dB. The quieter tubercled configurations also had a lower DPR. W40C20N5 had a mean DPR of 19.32 mm/rev, which was 1.12 mm/rev below the bare hull. This indicates a trade-off between noise and DPR, similar to the noise–efficiency trade-off of propellers reported by Knox et al. [12]. The influence of each design parameter is analysed in Section 5.3.

The within-configuration repeatability was high. The median CV of the hydrofoil configurations was 2.91% for velocity, 1.4% for RPS and 2.36% for DPR. The maxima were 10.49% for velocity and 3.70% for RPS, both for P170W20C20N0, and 9.18% for DPR, for P170W40C20N5. The CV of the 15 bare hull runs was 7.24% for velocity, 2.55% for RPS and 5.28% for DPR. A velocity CV below 2.46% was found for 13 configurations and a DPR CV below 2.46% for 16. The within-configuration standard deviation of L_p averaged 0.60 dB, with a median of 0.52 dB, compared with 1.71 dB among the 15 bare hull runs.

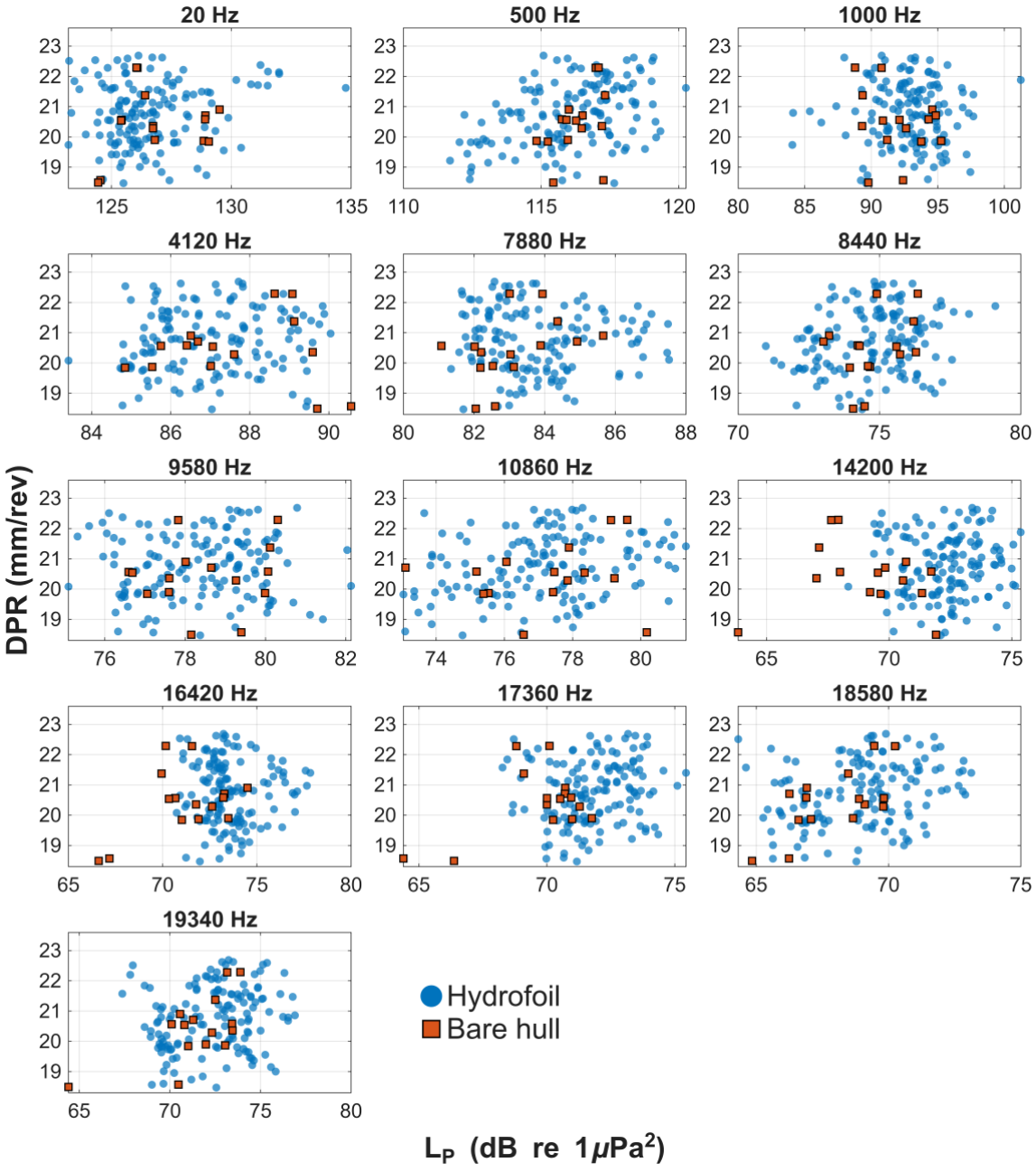


Figure 11. DPR and L_p data for hydrofoil and bare hull conditions at target frequencies.

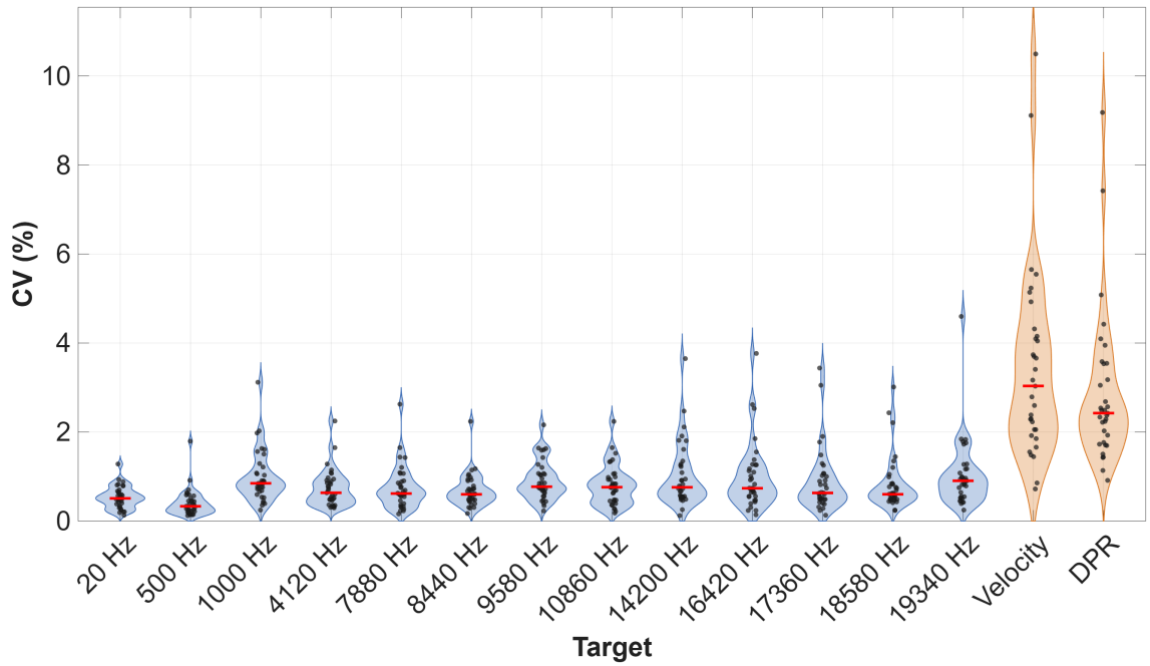


Figure 12. Violin plot with CV in each target parameter

5.3 The Importance and Impact of Design Parameters

The one-way ANOVA for each design parameter at the 13 target frequencies and for DPR is shown in Figure 13 with its F value. The analysis used the means of the 30 configurations, so that repeated runs of the same configuration were not treated as independent samples. The F value indicates the impact of a parameter: a larger F means that changing the parameter produces a larger difference between levels relative to the variation within levels. The p value indicates the reliability of this difference, and a threshold of 0.05 was applied. Filled markers show $p < 0.05$, where the effect was considered reliable, and hollow markers show $p \geq 0.05$. The critical F value at $p = 0.05$ is 4.20 for W and C, which are two-level targets; and 3.35 for P and N, the three-levels target. All filled markers lie to the right of these values and F values of different parameters cannot be compared directly.

Of the 56 tests, with 4 parameters in 14 targets, 9 were significant, whereas none was significant for P or N. No parameter reached significance at L_p targets for 20, 1000, 8440, 10860, 16420 and 17360 Hz or for DPR. The rest seven L_p frequencies had at least one significant parameter. W is significant in five targets, including 500, 7880, 9580, 18580 and 19340 Hz. It is maximum at 9580 Hz with F = 11.98. C is showed in four of 500, 4120, 9580 and 14200 Hz, maximum at

14200 Hz with F = 16.02. Notice in 500 Hz, both W and C were only marginally significant with F = 4.39 and p = 0.045.

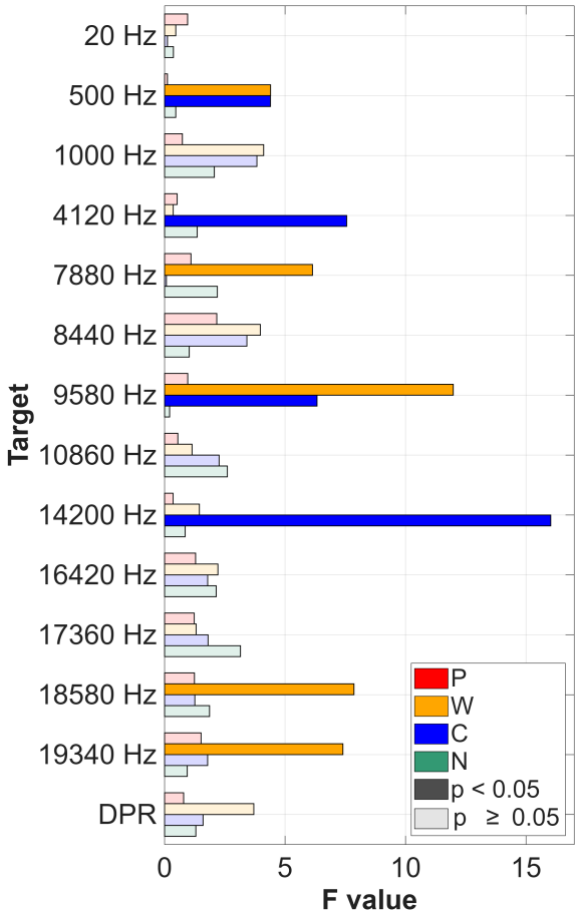


Figure 13. The ANOVA result on target frequencies and DPR with the four-design parameters: P (position), W (wingspan), C (chord length), N (tubercle numbers).

While the ANOVA measure the importance of the changes in design parameters, the net effect indicates their direction. For the seven frequencies target which showed significant in the ANOVA, they were carried into the net effect analysis, with their result displayed in Figure 14. It shows the net effect of each parameter after the other three parameters were removed. Each marker is the mean residual of one level, in dB, and the stars above the panels mark the pairwise differences between levels that were significant in a two-sample t-test with equal variances. "*" indicates the p value in t-test is less than 0.05, where "**" and "***" resulting in $p < 0.01$ and $p < 0.001$. Of the 56 pairwise comparisons, 11 were significant: 5 of 7 for W, 3 of 7 for C, 3 of 21 for N and 0 of 21 for P. P therefore showed no significant net effect at any frequency, which agrees with the ANOVA.

The direction of the effects depended on the parameter and the frequency. Increasing the chord length C from 20 to 40 mm raised L_p at all three significant frequencies, 1.54 dB at 4120 Hz, 1.32 dB at 14200 Hz and 0.76 dB at 9580 Hz. Increasing the wingspan from 20 to 40 mm lowered L_p at the three highest frequencies, which are 1.09 dB at 9580 Hz, 1.67 dB at 18580 Hz and 1.79 dB at 19340 Hz, but raised it at the two lower frequencies, as 0.85 dB at 4120 Hz and 1.03 dB at 7880 Hz. The effect of N was not monotonic. At 4120 Hz, the net effect of N = 0 was +0.7 dB and both N = 5 and N = 10 were lower by 1.26 dB and 1.09 dB, with no difference between N = 5 and N = 10. At 18580 Hz, N = 10 was 1.74 dB louder than N = 5 (p = 0.024), and N = 0 lay in between. N had no significant effect at 7880, 9580 or 14200 Hz.

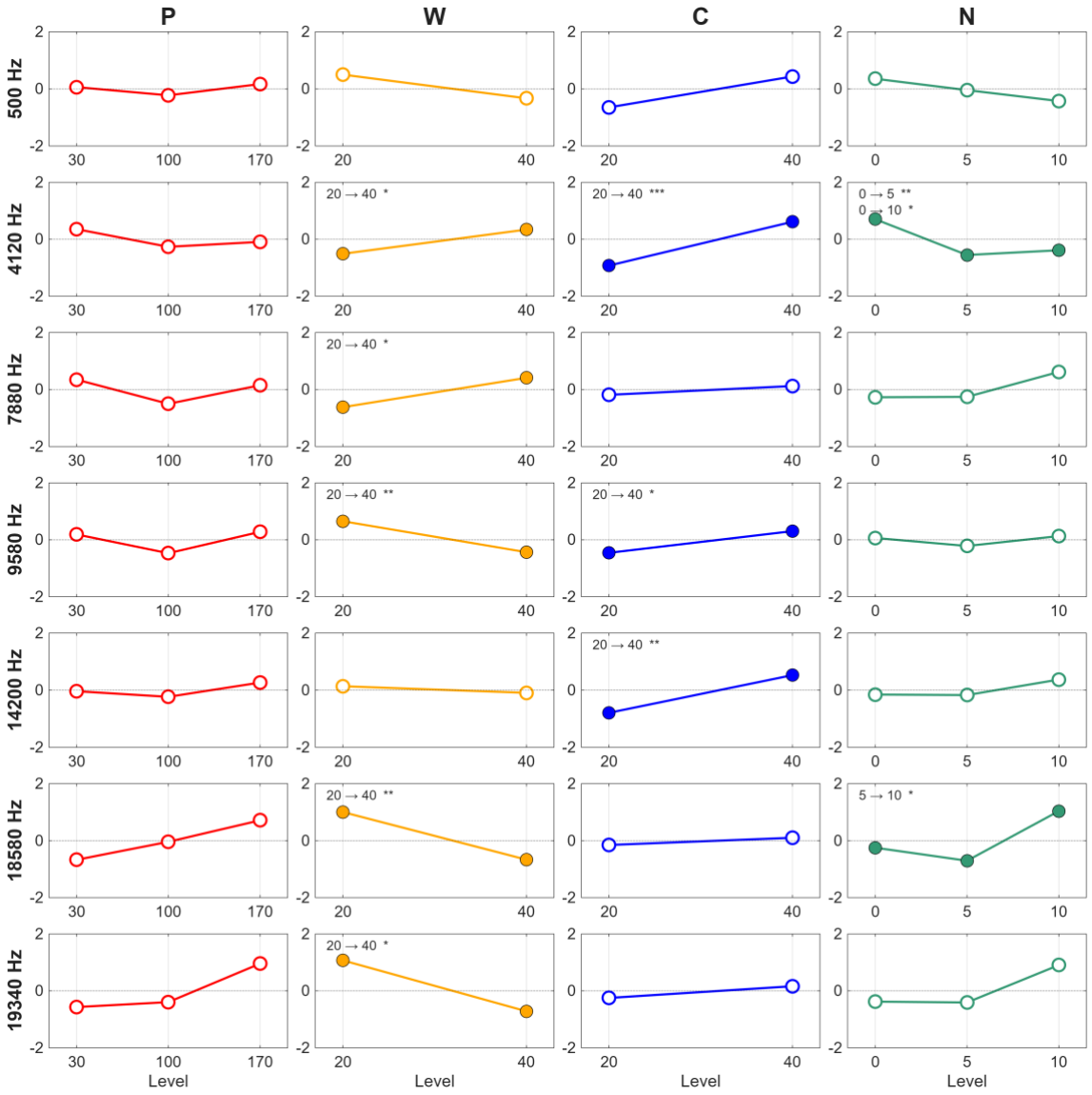


Figure 14. The net effect of the design parameters in dominated target frequencies

Comparing with previous studies, the dominance of C and W over P and N agrees with earlier studies showing that the effect of tubercles is governed by geometric ratios rather than by the presence of tubercles alone [7,10]. Wei et al. [10] highlighted the ratios of tubercle amplitude and wavelength to chord length for finite-span wings. In the present design the amplitude was fixed at 3 mm, so increasing C from 20 to 40 mm halved A/C from 0.15 to 0.075, while changing W altered the wavelength, defined as $\lambda = W/N$, and the span-to-chord ratio W/C. The lower L_p at 4120 Hz with tubercles of N = 5 and 10 than without tubercles at N = 0 is consistent with the reduced flow separation reported for tubercled hydrofoils [7,8]. At the highest frequencies, the two ways of increasing the amplitude-to-wavelength ratio A/λ, a smaller wingspan of W = 20 mm and a larger tubercle number of N = 10, both raised L_p at 18580 Hz, by 1.67 dB and 1.74 dB, respectively. This is consistent with the finding of Wei et al. [8,9] that a larger A/λ reduces flow separation but makes the flow more unsteady, which may add high-frequency noise. The present data cannot confirm this mechanism, and it does not explain why a larger W raised L_p at 4120 and 7880 Hz. The dependence of the effects on frequency is also similar to the dependence on operating condition reported for tubercled propellers, where the benefit appeared only at low tip speed ratios [16] and the penalty grew with advance ratio [15]. However, these studies measured forces or flow fields, not noise, at Reynolds numbers of $Re=1.4 \times 10^4$ to $Re=5 \times 10^5$ [7,8,10] , whereas the Reynolds number based on chord length and model speed was about $Re=4 \times 10^3$ to $Re=9 \times 10^3$ here, and the hydrofoil operated in the hull wake, so the comparison is qualitative. No previous study varied the position of a LET hydrofoil ahead of a propeller, so the non-significant effect of P has no direct reference. The effect of N also refers to the three W–C combinations at which N = 5 and 10 were tested, as described in Section 2.

6. Conclusions

This study experimentally investigated the acoustic and vessel advance performance of smooth and leading-edge-tubercled hydrofoils installed upstream of the propeller of a KVLCC2-type model tanker. Thirty configurations were evaluated over 147 runs by varying mounting position, wingspan, chord length and tubercle number. Comparisons with a bare-hull reference identified

opportunities for performance improvement, together with substantial dependence on hydrofoil geometry and the performance measure considered.

Across the tested configurations, the largest observed reduction in sound pressure spectral density level at an individual target frequency was 7.03 dB, equivalent to approximately an 80.2% reduction in pressure power spectral density at that frequency. The highest configuration-mean DPR was 22.03 mm/rev, representing a 7.8% increase over the bare-hull value of 20.44 mm/rev. These extrema describe separate acoustic and advance-performance outcomes and do not establish simultaneous improvements of these magnitudes in one configuration. The acoustic reduction is frequency-specific, while the DPR increase indicates greater advance per propeller revolution rather than a measured improvement in fuel consumption or propulsive efficiency.

Performance improvements were not consistent across the tested configurations. The mean spectral-level offset across the 13 selected frequency bands ranged from −1.07 to +3.17 dB relative to the bare hull, while configuration-mean DPR ranged from 18.40 to 22.03 mm/rev. Thus, some hydrofoils increased measured pressure spectral levels or reduced vessel advance performance. Although individual configurations offered favourable compromises, none demonstrated a consistent advantage across both performance measures and all selected frequency bands. The variability of the bare-hull measurements further requires the observed gains to be interpreted as candidates for confirmation under more closely controlled conditions.

The effect of tubercles depended strongly on the underlying hydrofoil geometry. For a wingspan of 40 mm and a chord of 20 mm, adding five tubercles lowered the mean spectral level by 1.85 dB relative to the corresponding smooth hydrofoils, averaged across mounting positions. At a chord of 40 mm, the same tubercle number instead increased the mean spectral level by 1.17 dB. Moreover, the quieter short-chord, five-tubercle configurations had a mean DPR of 19.32 mm/rev, 5.5% below the bare-hull reference. These contrasting responses show that tubercles cannot be treated as a uniformly beneficial addition and that acoustic benefits must be assessed alongside their effects on vessel advance performance. The exploratory one-way ANOVA identified chord length and wingspan as influential factors at selected frequencies, but detected

no significant main effects on DPR; these statistical findings remain subject to the incomplete factorial design and uncorrected multiple comparisons.

Further work should establish the repeatability of the most promising configurations using controlled operating conditions and interleaved reference tests. Completing the factorial design and varying tubercle amplitude would help resolve geometric interactions, while flow-field and load measurements are needed to explain how the hydrofoils modify propeller inflow and pressure fluctuations. Measurements of propulsion power at matched vessel speeds, together with acoustic measurements that distinguish local pressure fluctuations from radiated sound, would determine whether the observed model-scale benefits translate into energy savings and broader noise reductions. The present results therefore provide a basis for further optimisation of upstream hydrofoils, with acoustic and advance-performance objectives considered jointly.

Acknowledgements

This work is part of a project that has received funding from the EPSRC UK National Clean Maritime Research Hub (EP/Y024605/1).

Data availability

All data underlying the results are available as part of the article and no additional source data are required.

References

[1] International Maritime Organisation. Guidelines for the reduction of underwater noise from commercial shipping to address adverse impacts on marine life. International Maritime Organization 2014. https://wwwcdn.imo.org/localresources/en/OurWork/PartnershipsProjects/Documents/GloNoise-Library/MEPC.1-Circ.833-7April2014.pdf (accessed August 17, 2026).

[2] International Maritime Organisation. 2023 IMO Strategy on Reduction of GHG Emissions from Ships. International Maritime Organization 2023. https://www.imo.org/en/ourwork/environment/pages/2023-imo-strategy-on-reduction-of-ghg-emissions-from-ships.aspx (accessed August 1, 2026).

[3] International Maritime Organisation. Revised Guidelines for the Reduction of Underwater Radiated Noise from Shipping to Address Adverse Impacts on Marine Life. International Maritime Organization 2024. https://wwwcdn.imo.org/localresources/en/MediaCentre/Documents/MEPC.1-Circ.906-Rev.1%20-%20Revised%20Guidelines%20For%20The%20Reduction%20Of%20Underwater%20Radiated.pdf (accessed August 17, 2026).

[4] Fish FE, Weber PW, Murray MM, Howle LE. The Tubercles on Humpback Whales' Flippers: Application of Bio-Inspired Technology. Integr Comp Biol 2011;51:203–13. https://doi.org/10.1093/icb/icr016.

[5] Wikimedia Commons, 2026. (accessed November 07, 2026).

[6] Watts P, Fish FE. The Influence of Passive, Leading Edge Tubercles on Wing performance. 2001.

[7] Fan M, Dong X, Li Z, Sun Z, Feng L. Numerical and experimental study on flow separation control of airfoils with various leading-edge tubercles. Ocean Engineering 2022;252. https://doi.org/10.1016/j.oceaneng.2022.111046.

[8] Wei Z, New TH, Cui YD. An experimental study on flow separation control of hydrofoils with leading-edge tubercles at low Reynolds number. Ocean Engineering 2015;108:336–49. https://doi.org/10.1016/j.oceaneng.2015.08.004.

[9] Wei Z, Zang B, New TH, Cui YD. A proper orthogonal decomposition study on the unsteady flow behaviour of a hydrofoil with leading-edge tubercles. Ocean Engineering 2016;121:356–68. https://doi.org/10.1016/j.oceaneng.2016.05.043.

[10] Wei Z, Toh JWA, Ibrahim IH, Zhang Y. Aerodynamic characteristics and surface flow structures of moderate aspect-ratio leading-edge tubercled wings. Eur J Mech B Fluids 2019;75:143–52. https://doi.org/10.1016/j.euromechflu.2019.01.001.

[11] Kimmerl J, Abdel-Maksoud M. Visualization of Underwater Radiated Noise in the Near- and Far-Field of a Propeller-Hull Configuration Using CFD Simulation Results. J Mar Sci Eng 2023;11. https://doi.org/10.3390/jmse11040834.

[12] Knox B, Dylejko P, Chen L, Skvortsov A. Mapping Noise and Efficiency for Marine Propeller Designs. Proceedings of Acoustics 2016 2016.

[13] Tani G, Viviani M, Hallander J, Johansson T, Rizzuto E. Propeller underwater radiated noise: A comparison between model scale measurements in two different facilities and full scale measurements. Applied Ocean Research 2016;56:48–66. https://doi.org/10.1016/j.apor.2016.01.007.

[14] International Towing Tank Conference. ITTC - Recommended Procedures and Guidelines. International Towing Tank Conference 2021.

[15] Stark C, Shi W, Atlar M. A numerical investigation into the influence of bio-inspired leading-edge tubercles on the hydrodynamic performance of a benchmark ducted propeller. Ocean Engineering 2021;237. https://doi.org/10.1016/j.oceaneng.2021.109593.

[16] Shi W, Rosli R, Atlar M, Norman R, Wang D, Yang W. Hydrodynamic performance evaluation of a tidal turbine with leading-edge tubercles. Ocean Engineering 2016;117:246–53. https://doi.org/10.1016/j.oceaneng.2016.03.044.

[17] American Bureau of Shipping. Underwater Noise and External Airborne Noise. 2024.

[18] Liu J, Hu L, Zhang B, Zhang K, Bi J, Zheng Q. Enhancing ship hydrodynamic performance via machine learning-driven CFD parametric optimization. Engineering Applications of Computational Fluid Mechanics 2025;19. https://doi.org/10.1080/19942060.2025.2565801.

[19] Atlar M, Seo K, Sampson R, Danisman DB. Anti-slamming bulbous bow and tunnel stern applications on a novel Deep-V catamaran for improved performance. International Journal of Naval Architecture and Ocean Engineering 2013;5:302–12. https://doi.org/10.2478/IJNAOE-2013-0134.

[20] Kim I-T, Kim C, Kim S-H, Ko D, Moon S-H, Park H, et al. Estimation of the manoeuvrability of the KVLCC2 in calm water using free running simulation based on CFD. International Journal of Naval Architecture and Ocean Engineering 2021;13:466–77. https://doi.org/10.1016/j.ijnaoe.2021.05.004.

[21] Simman. KVLCC2. Simman2020 2020. https://simman2020.kr/contents/KVLCC2.php (accessed June 16, 2026).

[22] Simman. MOERI Tanker KVLCC2. Webmaster@simman2008Dk 2008. http://www.simman2008.dk/kvlcc/kvlcc2/kvlcc2_geometry.html (accessed June 16, 2026).

[23] Montgomery DC. Design and Analysis of Experiments. 9th ed. Wiley; 2017.